Implicit Model Predictive Control of a Full Bridge DC–DC Converter

Yanhui Xie, *Senior Member, IEEE*, Reza Ghaemi, Jing Sun, *Fellow, IEEE*, and James S. Freudenberg, *Fellow, IEEE*

***Abstract*—This paper presents a model predictive control (MPC)-based approach for a full bridge dc–dc converter of a fuel cell power system. The objective of the proposed control algorithm is to regulate the output voltage without violating the peak current constraint. We first develop a large signal dynamic model for the full bridge dc–dc converter. The peak current protection requirement is then formulated as a mixed input and state constraint for the MPC scheme. We next introduce the integrated perturbation analysis and sequential quadratic programming (InPA-SQP) method to solve the constrained optimal control problem with submillisecond level sampling time. The InPA-SQP solver can meet the computational efficiency demand, thereby enabling implementation of an implicit MPC for power electronics system with fast dynamics. The effectiveness of the proposed control algorithm in the peak current protection and the output voltage regulation has been verified with experimental results.**

***Index Terms*—Full bridge dc–dc converter, InPA-SQP, model predictive control, nonlinear constraint, peak current protection.**

I. Introduction

FUEL cells have shown great potential for various applications as a low emission and high-efficiency power source [1]. They are characterized as a low-voltage high-current power source whose output voltage varies for different loads, thereby necessitating a dedicated power conditioning system to regulate the dc output voltage. To investigate the voltage regulation of a fuel cell power system, an experimental testbed was developed at the University of Michigan to support model development and to facilitate a model based control design approach. Fig. 1 depicts the configuration of the power stage of the testbed, which is composed of a full bridge dc–dc converter and a polymer electrolyte membrane (PEM) fuel cell emulator, where $D_1 - D_4$ are the corresponding anti-parallel diodes of the power switches $Q_1 - Q_4$ while $D_5 - D_8$ form the output rectifier, L is the leakage inductance of the transformer with turn ratio n, C_1 and C_o are the input and output capacitor, respectively, R is the load, and V_1 and V_o are the input voltage and the output voltage, respectively. The ac side of each bridge is connected to the transformer with corresponding primary voltage V_{ac1} and secondary voltage V_{ac2}, respectively. Parameters of the full bridge dc–dc converter are shown in Table I.

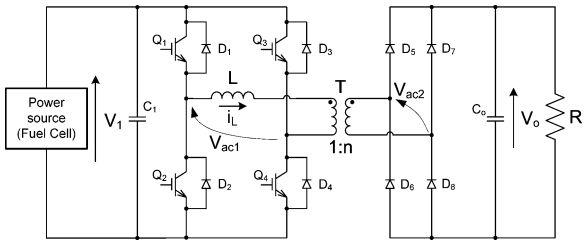

Fig. 1. Full bridge dc–dc converter-based fuel cell power system.

TABLE I
PARAMETERS OF THE TESTBED PROTOTYPE

Item	Parameter
Inductor L	$10.5\mu H$
Capacitor C_o	$1410\mu F$
Transformer turn ratio n	2
Switching period T	$100\mu s$
V_1 (nominal)	$60V$
Desired V_o	$80V$
Nominal load R	6.4Ω
Rated power	$1000W$

The full bridge topology was initially proposed in previous papers [2] and [3] for both high power density and high power applications. It is very attractive because of its zero voltage switching, low component stresses, and high power density features. Moreover, its high frequency transformer prevents fault propagation and enables a high output–input voltage ratio. Therefore, with a full bridge dc–dc converter as the power conditioning system, the fuel cell power system can be applied to high dc voltage applications, such as the dc zonal electrical distribution system of an all-electric ship [4]. As a power converter with 10 kHz switching frequency, its time constant is at the millisecond level. Given that the time constant for a PEM fuel cell is about several seconds [5], there is a significant time scale separation between the dynamics of the fuel cell and the power converter. This fact suggests that we can design controllers for the fuel cell and the power converter separately without substantial performance degradation. The control design for a PEM fuel cell system has been extensively addressed, see, (e.g., [6]–[8]). The main goal of this paper is to design a controller for the full bridge dc–dc converter.

Several challenges arise for the dc–dc converter control design. First, the power devices of the dc–dc converters have very complicated time-varying switching behavior, which defines the shape of the inductor current, making the dynamic model development of power converters a challenge. Second,

Manuscript received February 27, 2009; revised June 25, 2009. Current version published December 28, 2009. Recommended for publication by Associate Editor B. Lehman. This work was supported by the U.S. Office of Naval Research (ONR) under Grants N00014-08-1-0611 and N00014-05-1-0533.

The authors are with the Department of Electrical Engineering and Computer Science and the Department of Naval Architecture and Marine Engineering, University of Michigan, Ann Arbor, MI 48109 USA (e-mail: yhxie@umich.edu; ghaemi@umich.edu; jingsun@umich.edu; jfr@eecs.umich.edu).

Color versions of one or more of the figures in this paper are available online at http://ieeexplore.ieee.org.

Digital Object Identifier 10.1109/TPEL.2009.2030196

dc–dc converters for fuel cell power systems have a wide range of operating conditions, further complicating the control design. Furthermore, the control input is bounded due to physical limitations of power converters. Finally, safe operation requirements such as peak current limitation may impose additional nonlinear constraints.

Traditionally, there are two classes of algorithms for dc–dc converter control, namely the voltage mode control and current mode control [9]–[12]. Voltage mode control achieves voltage regulation through a single-loop voltage control scheme. To limit the current during transient operation within safe operation range, the feedback control gain must be carefully chosen, otherwise an additional protection circuit has to be incorporated. Current mode control includes two subclasses, namely the average current control and peak current control. In addition to a voltage feedback loop, current mode control employs an inner inductor current feedback loop to improve performance. Performance enhancements, including superb line regulation and inherent over-current protection, can be achieved for current mode control. However, current mode control has a subharmonic oscillation problem when the duty ratio is greater than 0.5 [13]. Besides, this method requires inductor current sensing, which increases system cost and tends to have noise sensitivity problems. The development of advanced control algorithms, together with the increased computational power of microprocessors, enables us to deal with the control problem from a new perspective. For example, one step predictive control based algorithms are applied to power electronics system, (see, e.g., [14] and [15]) while model predictive control (MPC) has been implemented in an electric drive system for direct torque control [16] and [17] and in a flying capacitor converter [18]. For the full bridge dc–dc converter under investigation, the peak current protection problem can be formulated as a constraint for an optimal control problem, which can be effectively dealt with using MPC.

MPC, also known as receding horizon control, combines optimization with feedback control for systems subject to input and state constraints [19]–[21]. In classical MPC, the control action at each time step is obtained by solving an online optimization problem with a given cost function. However, solving an optimization problem is often computationally demanding, which contributes to the fact that most of successful applications have been found for systems with slow dynamics and abundant computational power. For systems with fast dynamics, explicit MPC [22] and [23] has been proposed that precomputes the optimal solutions and stores them for online lookup. Explicit MPC has been implemented for fast dynamic applications with a millisecond level time constant [24]. The major challenge of implementing explicit MPC is that the number of entries in the lookup table could be very large, thereby limiting its application to small problems with low dimensions [25].

To extend the applicability of MPC to broader classes of systems with fast dynamics, a novel numerical optimization algorithm is developed to improve computational efficiency. This algorithm is referred to as the integrated perturbation analysis and sequential quadratic programming (InPA-SQP) solver [26], [27]. It combines the computational advantages of perturbation analysis and optimality of the SQP solution by treating the optimization problem at time k as a perturbed problem at time $k-1$. This combination can significantly improve computational efficiency and is particularly useful for MPC, where an optimal control problem must be solved repeatedly over the receding horizon. It is worthwhile to point out that the InPA-SQP algorithm can be applied to solve the MPC optimal control problem for nonlinear systems with mixed state and control input constraints.

This paper is concerned with the dc–dc converter control using the MPC scheme. We first analyze the operation of the full bridge dc–dc converter shown in Fig. 1. A large signal dynamic model is then developed for the full bridge dc–dc converter, based on which a nonlinear observer is designed. The observer provides the feedback of the inductor current without using a current sensor, leaving the output voltage V_o to be the only measured state. We next formulate the voltage regulation problem as an MPC problem with a nonlinear constraint that captures the peak current protection requirement. To achieve the sub-millisecond level sampling time and handle the nonlinear constraint, the InPA-SQP method is introduced to solve the constrained optimal control problem. The InPA-SQP solver can significantly improve computational efficiency while effectively handling the nonlinear constraints, making the implicit MPC feasible for a power electronics system with very fast dynamics. The effectiveness of the proposed control algorithm in achieving the peak current protection has been verified with experimental results.

The rest of this paper is organized as follows. In Section II, the operation analysis of the full bridge dc–dc converter will be presented. Section III is devoted to the development of a large signal dynamic model and a nonlinear observer for the full bridge dc–dc converter. Section IV focuses on MPC problem formulation while Section V will be devoted to the InPA-SQP solver interpretation. Experimental results will be presented in Section VI, followed by conclusions in Section VII.

II. Operation Analysis of the DC–DC converter

To understand the characteristics of the full bridge dc–dc converter, we start with an analysis of its operation using techniques similar to those presented in [28]–[30]. The full bridge dc–dc converter is typically modulated by the phase shift modulation signals $V_{Q_1} \sim V_{Q_4}$ shown in Figs. 2(a) and 3(a), where $\beta \in [0,1]$ is the normalized phase shift between the two half bridges composed of Q_1/Q_2 and Q_3/Q_4, respectively. Note that since the parallel resistance and inductance are much greater than the series resistance and inductance, the equivalent circuit model of a high frequency transformer can be simplified as an ideal transformer with a primary series inductor (leakage inductor). Therefore, the electrical connection between V_{ac1} and V_{ac2} shown in Fig. 1 can be expressed by the simplified diagram shown in Fig. 4, where L is the leakage inductance. By shifting the phase between the two half bridges, different combinations of V_{ac1} and V_{ac2} can be applied to shape the current i_L and consequently to manipulate the power flow. Based on the shape of i_L, there are two operation modes for the full bridge converter, namely the discontinuous-conduction-mode (DCM) and

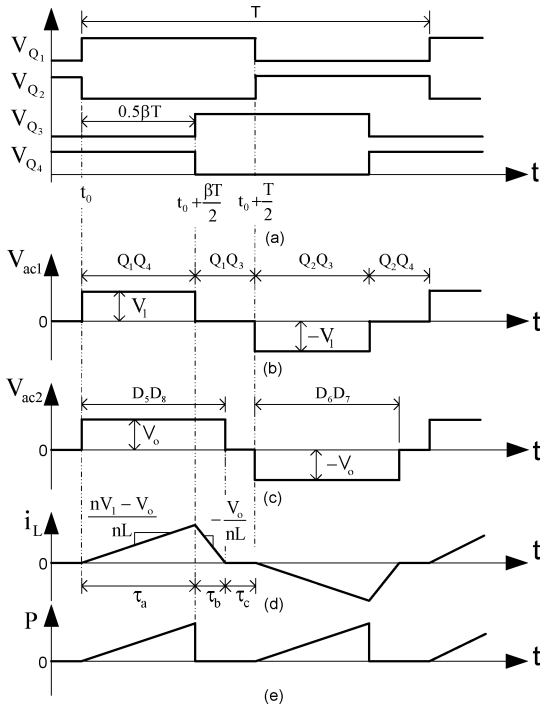

Fig. 2. Modulation sequence and ideal waveforms of the full bridge dc–dc converter for DCM.

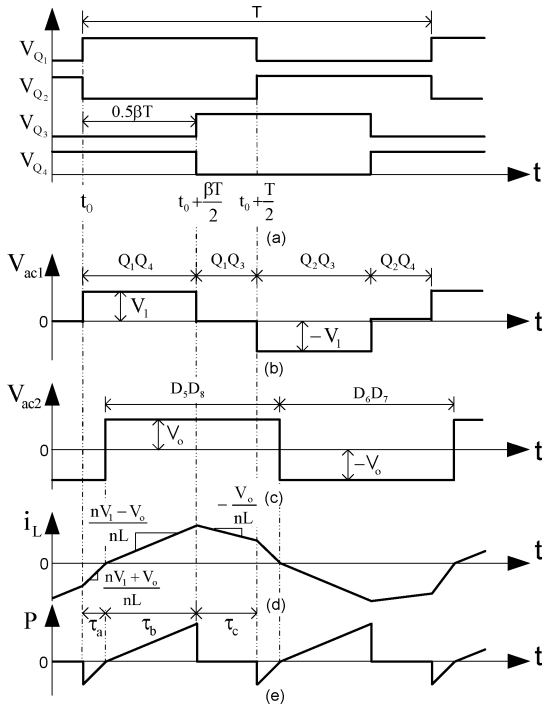

Fig. 3. Modulation sequence and ideal waveforms of the full bridge dc–dc converter for CCM.

the continuous-conduction-mode (CCM). DCM refers to the case that the inductor current i_L stays at zero for a certain period of time for each half switching cycle as shown in Fig. 2(d). CCM means that the inductor current i_L only crosses zero but never stays at zero for each half switching period as shown in Fig. 3(d). For each operating mode, the half switching cycle $[t_0, t_0 + (T/2)]$ can be divided into three segments according to the evolution of i_L. The three segments have corresponding time intervals τ_a, τ_b, and τ_c, respectively, as illustrated in Figs. 2(d) and 3(d). The goal of this analysis is to determine the operation boundary between DCM and CCM, and obtain the current and power characteristics for each operating mode.

A. DCM Operation

For a full bridge dc–dc converter operating with DCM, the ideal voltage waveforms of $V_{\rm ac1}$ and $V_{\rm ac2}$ are shown in Fig. 2(b) and (c). The voltage across the inductor is $V_L = (V_{\rm ac1} - V_{\rm ac2})/n$, leading to the ideal inductor current i_L slope at each segment shown in Fig. 2(d).

Since we know the inductor current slopes and $\tau_a = \beta T/2$, the following relationship can be easily obtained:

$$\tau_b = \frac{(nV_1 - V_o)}{V_o}\tau_a = \frac{(nV_1 - V_o)\beta T}{2V_o} \tag{1}$$

$$\tau_c = \frac{T}{2} - \tau_a - \tau_b. \tag{2}$$

The peak current equals $i_L(t_0 + (\beta T/2))$ and can be calculated as

$$i_L\left(t_0 + \frac{\beta T}{2}\right) = \frac{(nV_1 - V_o)\beta T}{2nL}. \tag{3}$$

The average inductor current and average input power over the half switching cycle are

$$\bar{i}_L = \frac{2}{T}\int_{t_0}^{t_0+T/2} i_L\, dt = \frac{\beta^2 T V_1(nV_1 - V_o)}{4LV_o} \tag{4}$$

$$\overline{P} = \frac{2}{T}\int_{t_0}^{t_0+T/2} V_{\rm ac1} i_L\, dt = \frac{\beta^2 T V_1(nV_1 - V_o)}{4nL}. \tag{5}$$

B. CCM Operation

For a full bridge dc–dc converter operating with CCM, the voltage waveforms of $V_{\rm ac1}$ and $V_{\rm ac2}$ are shown in Fig. 3(b) and (c). The voltage across the inductor is $V_L = (V_{\rm ac1} - V_{\rm ac2})/n$, leading to the inductor current i_L slope at each segment shown in Fig. 3(d).

Given the inductor current slopes, one can easily obtain

$$\frac{(nV_1 + V_o)\tau_a}{nL} + \frac{V_o\tau_c}{nL} = \frac{(nV_1 - V_o)\tau_b}{nL} \tag{6}$$

$$\tau_b = \frac{\beta T}{2} - \tau_a. \tag{7}$$

Since $\tau_c = (1 - \beta)T/2$, solving (6) and (7) yields

$$\tau_a = \frac{(nV_1\beta - V_o)T}{4nV_1} \tag{8}$$

$$\tau_b = \frac{(nV_1\beta + V_o)T}{4nV_1}. \tag{9}$$

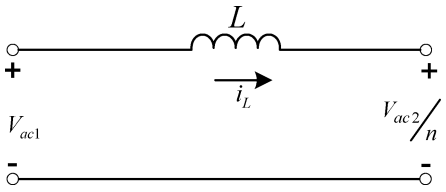

Fig. 4. Simplified dc–dc converter scheme.

The peak current equals $i_L(t_0 + (\beta T/2))$ and can be calculated as

$$i_L\left(t_0 + \frac{\beta T}{2}\right) = \frac{(nV_1 - V_o)(V_o + nV_1\beta)T}{8nLV_1}. \tag{10}$$

The average input power over the half switching cycle is

$$\overline{P} = \frac{2}{T}\int_{t_0}^{t_0+T/2} V_{\mathrm{ac1}} i_L \, dt = \frac{TV_o(2n^2V_1^2\beta - n^2V_1^2\beta^2 - V_o^2)}{8n^3LV_1}. \tag{11}$$

The operation mode of the dc–dc converter is determined by V_1, V_o, and β. For different combinations of V_1 and V_o, the phase shift boundary line $L_{\beta b}$ between the CCM and DCM can be calculated as follows, if we set $\tau_c = 0$ for DCM

$$L_{\beta b} = \left\{(\beta, V_1, V_o)|\beta = \frac{V_o}{nV_1}\right\}. \tag{12}$$

Moreover, let i_{peak} denotes the maximum tolerable peak current of the converter. Using (3) and (10), one can determine the limits on the phase shift to avoid over-peak-current. If the converter operates with CCM, the phase shift constraint curve $L_{\beta c}$ can be calculated from (10) as follows:

$$L_{\beta c} = \left\{(\beta, V_1, V_o)|\beta = \frac{8Li_{\mathrm{peak}}}{T(nV_1 - V_o)} - \frac{V_o}{nV_1}\right\}. \tag{13}$$

Similarly, if the converter operates with DCM, the phase shift constraint curve $L_{\beta d}$ can be calculated from (3) as follows:

$$L_{\beta d} = \left\{(\beta, V_1, V_o)|\beta = \frac{2nLi_{\mathrm{peak}}}{T(nV_1 - V_o)}\right\}. \tag{14}$$

Fig. 5 shows the phase shift boundary line $L_{\beta b}$ and the peak current constraint curves $L_{\beta d}$ and $L_{\beta c}$ for $V_1 = 60$ V and $V_o = 0V \sim 90V$. Note that: 1) the full bridge dc–dc converter operates with the CCM if the phase shift is larger than the corresponding boundary value, and 2) the peak current constraint curves $L_{\beta d}$ and $L_{\beta c}$ are calculated using (13) and (14) for $i_{\mathrm{peak}} = 75A$. Fig. 6 shows the power curve of the full bridge dc–dc converter for $V_1 = 60$ V and $V_o = 80$ V. For our system with a nominal output power of 1000 W, the phase shift at the nominal operating point is 0.62, which is smaller than the boundary value 0.67. Therefore, the converter operates with the DCM at steady state for the nominal output power. From Fig. 5, the DCM peak current constraint curve $L_{\beta d}$ is always above the boundary line $L_{\beta b}$, so, the peak current constraint will not be violated if the power converter operates with DCM at steady state. However, for the cases of starting process and overload, the power converter operates at CCM, where the CCM peak current constraint may be violated. Therefore, an active constraint

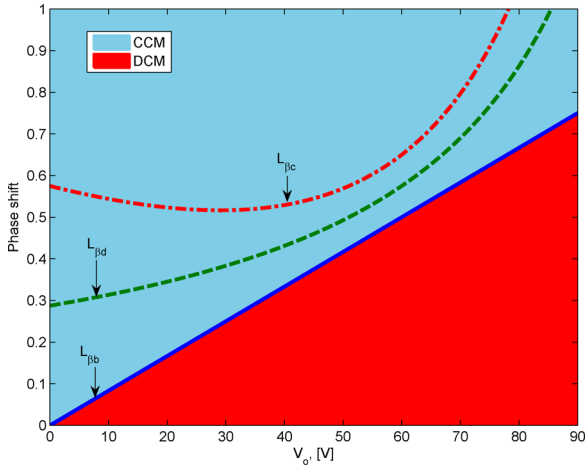

Fig. 5. DCM–CCM boundary line $L_{\beta b}$ and peak current constraint curves $L_{\beta d}$ and $L_{\beta c}$ for $V_1 = 60$ V and $i_{\mathrm{peak}} = 75$ A.

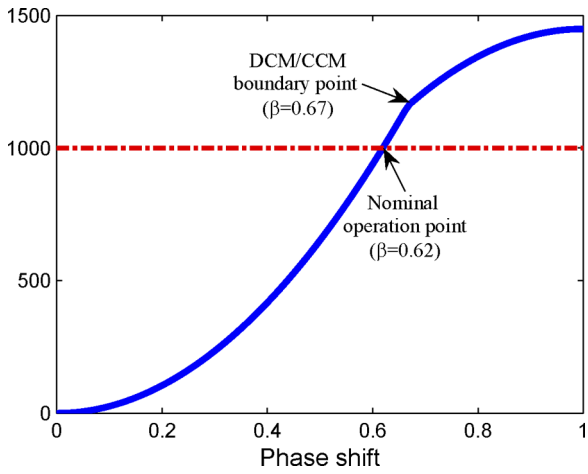

Fig. 6. Power curve of the full bridge dc–dc converter for $V_1 = 60$ V and $V_o = 80$ V.

enforcement mechanism needs to be incorporated to protect the converter.

III. Dynamic Model Development and Observer Design

Given the challenges imposed by the control of power converters, it is desirable to employ a model based control design approach to achieve satisfactory closed loop system performance. Since the full bridge dc–dc converter has a wide operating range, it is necessary to derive a large signal dynamic model for the system to facilitate the model based control design. For this work, an averaged dynamic model as developed for other power converters [31]–[33] is needed for control design. Using the analysis results presented in the previous section and following the same technique in [32], the dynamic model of the full bridge dc–dc converter can be derived as

$$\frac{d\bar{i}_L}{dt} = \frac{\beta V_1}{L} - \frac{4\bar{i}_L\bar{V}_o}{\beta T(nV_1 - \bar{V}_o)} \tag{15}$$

$$\frac{d\bar{V}_o}{dt} = \frac{\bar{i}_L}{nC_o} - \frac{\bar{V}_o}{RC_o} \tag{16}$$

$$y = \bar{V}_o. \tag{17}$$

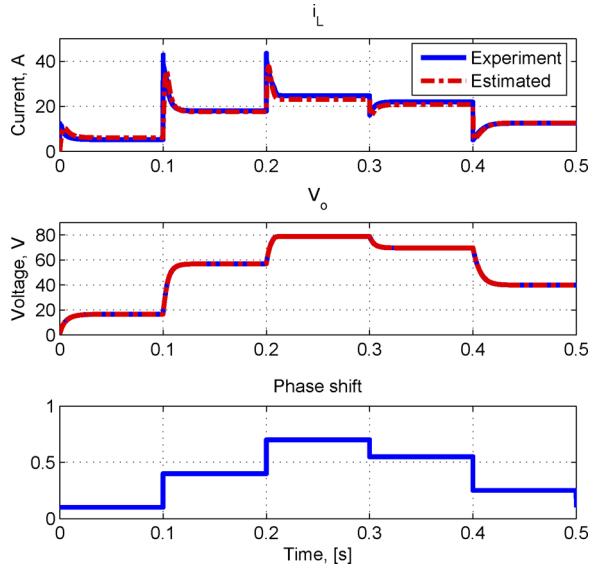

Fig. 7. Comparison of estimated and measured states.

Note that $\bar{i}_L$ and $\bar{V}_o$ represent the average current and the average output voltage over a switching period.

For the dynamic system represented by (15)–(17), the implementation of advanced control strategies requires a current sensor to obtain the average current $\bar{i}_L$ for state feedback. On one hand, the current sensor must have high bandwidth to accurately reconstruct the current signal. On the other hand, due to electromagnetic interference, it is often necessary to use a low-pass filter to remove noise. However, a low-pass filter typically introduces additional phase lag for the closed loop system. To overcome these drawbacks, we propose to use a nonlinear observer to estimate the average current $\bar{i}_L$ while keeping the voltage $\bar{V}_o$ as the only measured variable. The nonlinear observer is expressed as follows:

$$\frac{d\hat{\bar{i}}_L}{dt} = \frac{\beta V_1}{L} - \frac{4\hat{\bar{i}}_L\hat{\bar{V}}_o}{\beta T(nV_1 - \hat{\bar{V}}_o)} + H_1(y-\hat{y}) \tag{18}$$

$$\frac{d\hat{\bar{V}}_o}{dt} = \frac{\hat{\bar{i}}_L}{nC_o} - \frac{\hat{\bar{V}}_o}{RC_o} + H_2(y-\hat{y}) \tag{19}$$

$$\hat{y} = \hat{\bar{V}}_o. \tag{20}$$

To properly select the gains H_1 and H_2 for the nonlinear observer, we linearize the plant at the desired operating point. The faster eigenvalue of the linearized model is around -800. We chose $H_1 = 2759$ and $H_2 = 2859$ to place the eigenvalues of the observer at -2000 to achieve fast convergence of the observer.

Fig. 7 compares the estimated states with the actual measured states. The observed states closely track the real states for different operating points. This figure also confirms the accuracy of the nonlinear model.

IV. MPC FORMULATION

This section presents the formulation of the MPC controller for the voltage regulation problem of the full bridge dc–dc converter. The dynamic system represented by (15)–(17) can be easily linearized with nominal value $x^o = [25, 80]^T$ and $u^o = 0.62$. Let $x_1 = \bar{i}_L - 25$, $x_2 = \bar{V}_o - 80$ and $u = \beta - 0.62$, the system can be transformed into its discrete-time version for a specific sampling time

$$x(k+1) = f(x(k), u(k)) := Ax(k) + Bu(k) \tag{21}$$

$$y(k) = Fx(k) \tag{22}$$

where $A \in \mathbb{R}^{n\times n}$, $B \in \mathbb{R}^{n\times m}$, $F \in \mathbb{R}^{m\times n}$. Note that $n = 2$ and $m = 1$ for the system under investigation.

For a given i_{peak}, the CCM peak current (10) must satisfy

$$\frac{(nV_1 - V_o)(V_o + nV_1 a)T}{8nLV_1} \le i_{\text{peak}}. \tag{23}$$

Equation (23) can be rewritten in terms the state variables as

$$E_1(x(k), u(k)) \le 0. \tag{24}$$

where

$$E_1(x(k), u(k)) = \frac{(nV_1 - (x_2^o + x_2(k)))((x_2^o + x_2(k)))}{V_1} + \frac{(nV_1 - (x_2^o + x_2(k)))(nV_1(u^o + u(k)))}{V_1} - \frac{8nLi_{\text{peak}}}{T}. \tag{25}$$

Then the MPC online optimization problem can be formulated as follows: at the time instant k, the state of the system $x(k)$ is observed and the following optimal control problem $\mathscr{P}_N(x(k))$ is solved

$$\mathscr{P}_N(x(k)) : V_N^*(x(k)) = \min_{\mathbf{u}}\{V_N(x(k), \mathbf{u})\} \tag{26}$$

$$V_N(x(k), \mathbf{u}) = \sum_{j=k}^{k+N-1} G(x(j), u(j)) + \Phi(x(N)) \tag{27}$$

subject to

$$x(j+1) = f(x(j), u(j)), \quad f : \mathbb{R}^{n+m} \to \mathbb{R}^n \tag{28}$$

$$x(0) = x(k) \in \mathbb{R}^n \tag{29}$$

$$E(x(\cdot), u(\cdot)) \le 0, \ E : \mathbb{R}^{n+m} \to \mathbb{R}^l \tag{30}$$

where

$$\mathbf{u} = \{u(k), u(k+1), \ldots, u(k+N-1)\} \tag{31}$$

is the control sequence

$$x(j) := x^{\mathbf{u}}(j; x(k)), j = k, k+1, \ldots, k+N-1 \tag{32}$$

is the state trajectory at time instant j resulting from an initial state $x(k)$ and the control sequence $\mathbf{u}$

$$G(x(j), u(j)) = x(j)^T Qx(j) + u(j)^T Wu(j), \quad j = k, k+1, \ldots, k+N-1 \tag{33}$$

and $\Phi(x(N))$ is the penalty for the final states. $Q \in \mathbb{R}^{n\times n}$ and $W \in \mathbb{R}^{m\times m}$ are the corresponding weighting matrices which are used to penalize the deviation of the output and the control input to their corresponding desired value, N is the prediction

horizon, and $E(x(k), u(k))$ is the constraint matrix and can be written as follows with $l = 3$:

$$\begin{bmatrix} u(j) - (1 - u^o) \\ -u(j) - u^o \\ E_1(x(j), u(j)) \end{bmatrix}. \quad (34)$$

Note that the first two components are derived because of the boundedness of the phase shift ($\beta \in [0, 1]$) and each component in (34) is bounded above by zero.

Since the full bridge dc–dc converter has the millisecond level time constant, a rational choice of the sampling time is between 100 and 400 μs [34]. The length of the prediction horizon N is a basic tuning parameter for MPC controllers. Generally speaking, the closed loop system performance improves as N increases. However, additional computational effort associated with a long horizon could be troublesome for implicit MPC of power electronics systems. We choose 150 μs as the sampling time for the controller and $N = 10$ as the prediction horizon. The weighting matrices Q and W are the main tuning parameters of the quadratic cost function (27) to shape the closed-loop response for desired performance. The closed loop performance criteria are defined as: 1) to achieve fast output response with small output overshoot; and 2) to avoid high frequency control input oscillation which might cause high slew rate for the inductor current and high stress for switching components. We evaluate the performance to different combinations of weighting matrix using a virtual hardware for controller tuning. The virtual hardware is developed using MATLAB/Simulink/SimPowerSystems toolbox and has the same parameters as the real hardware. The preliminary evaluation results lead to the choice of $Q = [0\ 0; 0\ 0.01]$ and $W = 1$. Furthermore, we do not penalize the final states $x(N)$, meaning $\Phi(x(N)) = 0$.

Given the fast dynamics of the converter, we have to apply fast algorithms to solve the above optimization problem online in real-time. This requirement motivates us to introduce the InPA-SQP method in Section V.

V. InPA-SQP Algorithm

We now introduce a method, which we refer to as the InPA-SQP approach [26] and [27], for the implicit MPC implementation.

According to the MPC strategy, at the time instant k, the state of the system $x(k)$ is observed and the optimal control problem $P_N(x(k))$ defined by (26)−(30) is solved. The resulting optimal control sequence is

$$\mathbf{u}^*(x(k)) = \{u^*(k; x(k)), u^*(k+1; x(k)), \ldots, u^*(k+N-1; x(k))\} \quad (35)$$

the optimal state trajectory is

$$\mathbf{x}^*(x(k)) = \{x^*(k; x(k)) := x(k), x^*(k+1; x(k)), \ldots, x^*(k+N; x(k))\} \quad (36)$$

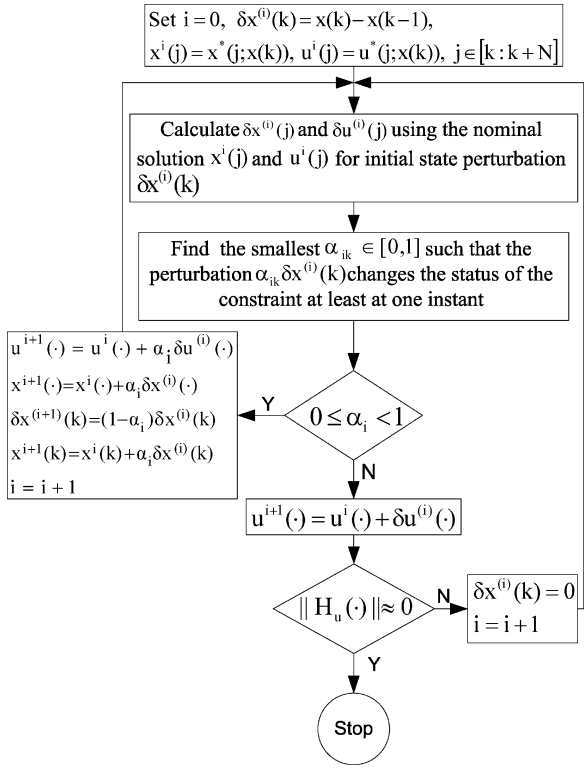

Fig. 8. Intermediate initial conditions which handle the large perturbation.

and the model predictive control law at the time instant k is defined as

$$h(x(k)) := u^*(k; x(k)). \quad (37)$$

According to InPA-SQP approach, the optimal solution at each time instant k for the observed state $x(k)$ is calculated using the optimal solution at the previous time instant, i.e., $k-1$. Given the optimal control sequence $\mathbf{u}^*(x(k-1))$, the updated optimal control sequence $\mathbf{u}^*(x(k))$ can be computed using perturbation analysis where the initial state is perturbed by $\delta x(k) = x(k) - x(k-1)$. If the variation $\delta x(k)$ in the initial state causes changes in the activity status of constraints, the variation is split into small variations, i.e., $\delta x^{(i)}(k),\ i = 1, 2, \ldots$, where for each incremental variation, only one constraint changes from active to inactive or vise versa. With these small variations, some intermediate points are identified along the line connecting $x(k-1)$ and $x(k)$. These intermediate points are denoted $x^{(0)}(k), x^{(1)}(k), \ldots, x^{(i_p)}(k)$ with $x^{(0)}(k) = x(k-1)$ and $x^{(i_p)}(k) = x(k)$, as shown in Fig. 8. Then the corresponding approximation of the optimal control sequence $\mathbf{u}^*(x^i(k)),\ i = 1, \ldots, i_p$ are calculated using perturbation analysis.

Note that the control sequence provided by perturbation analysis at each intermediate point $x^i(k)$, i.e., $\mathbf{u}^*(x^i(k))$ is an approximation to the optimal control sequence. Therefore, the error can accumulate and optimality condition may be lost at these intermediate steps. To compensate this error and maintain the optimality of the approximate solution, we use a special formulation of SQP with active set method to modify the perturbed

analysis algorithm. This special formulation allows us to cast the solution of the SQP into a formula which is similar to that of the perturbation analysis, thereby, facilitating the seamless integration of perturbation analysis and SQP to speed up the calculation of the optimal solution. The detailed algorithm is presented as follows for the general nonlinear MPC implementation.

At the time instant k, we need to solve $\mathscr{P}_N(x(k))$, given the solution of $P_N(x(k-1))$. We consider the general case where functions $G(x(\cdot),u(\cdot))$, $G:\mathbb{R}^{n+m}\to\mathbb{R}$, $\Phi(x(\cdot))$, $\Phi:\mathbb{R}^{n+m}\to\mathbb{R}$, $f(x(\cdot),u(\cdot))$, $E(x(\cdot),u(\cdot))$ are twice continuously differentiable with respect to x and u. Moreover, let us define the Hamiltonian function H at prediction time instants $k, k+1,\ldots,k+N-1$ as

$$H(j) := G(x(j),u(j)) + \lambda(j+1)^T f(x(j),u(j)) + \mu(j)^T E(x(j),u(j)),\ j=k,\ldots,k+N-1 \tag{38}$$

where, $\mu(j)$ is the Lagrange multiplier associated with the inequality constraint (30) and $\lambda(j+1)$ is the Lagrange multiplier associated with equality constraint (28) at the prediction time instant j, where $j>k$.

Since we know the solution of $P_N(x(k-1))$ at the time instant k, by treating the initial state $x(k)$ as $x(k-1)$ plus its perturbation $\delta x(k)=x(k)-x(k-1)$, we go through the following steps to calculate the optimal solution for the initial state $x(k)$.

1) Measure $x(k)$ and assume $\mathbf{u}^*(x(k-1))$ and $x(k-1)$ are given from previous time instant $k-1$.
2) Set $i=0$, $\delta x^{(0)}(k)=x(k)-x(k-1)$, $x^{(0)}(j)=x^*(j;x(k-1))$, and $u^{(0)}(j)=u^*(j;x(k-1))$, for $j=k,\ldots,k+N-1$.
3) Calculate the state and control variation $\delta x^{(i)}(j+1)$ and $\delta u^{(i)}(j)$, $j\in[k:k+N]$, for the initial state perturbation $\delta x^{(i)}(k)$, as follows:

$$\delta u^{(i)}(j) = -[I\ 0]K_0(j) \times \begin{bmatrix} Z_{ux}(j)\delta x^{(i)}(j) + f_u^T(j)T(j+1) + H_u(j) \\ E_x^a(j)\delta x^{(i)}(j) \end{bmatrix}$$

$$\delta x^{(i)}(j+1) = f_x(j)\delta x^{(i)}(j) + f_u(j)\delta u^{(i)}(j) \quad \text{and } \delta x^{(i)}(k) \text{ given} \tag{39}$$

where $H_u(j)$ is the partial derivative of the Hamiltonian function with respect to control u at the prediction time instant j, and

$$\begin{aligned} Z_{uu}(j) &= H_{uu}(j) + f_u^T(j)S(j+1)f_u(j) \\ Z_{ux}(j) &= Z_{xu}(j)^T = H_{ux}(j) + f_u^T(j)S(j+1)f_x(j) \\ Z_{xx}(j) &= H_{xx}(j) + f_x^T(j)S(j+1)f_x(j) \end{aligned} \tag{40}$$

with $S(j)$ being calculated by the following backward recursive equations

$$S(k+N)=\Phi_{xx}(k+N), T(k+N)=0$$

$$S(j) = Z_{xx}(j) - [Z_{xu}(j)\ E_x^{aT}(j)]K_0(j)\begin{bmatrix} Z_{ux}(j) \\ E_x^a(j) \end{bmatrix}$$

$$T(j) = f_x^T(j)T(j+1) - [Z_{xu}(j)\ E_x^{aT}(j)]K_0(j) \times \begin{bmatrix} f_u^T(j)T(j+1) + H_u(j) \\ 0 \end{bmatrix} \tag{41}$$

and when the constraint is active, $K_0(\cdot)$ is given by

$$K_0(j) = \begin{bmatrix} Z_{uu}(j) & E_u^{aT}(j) \\ E_u^a(j) & 0 \end{bmatrix}^{-1} \tag{42}$$

where $E^a(j)$ is a vector consisting of those elements of the vector $E(x(j),u(j))$ whose corresponding inequality constraints are active. If no constraint is active at the prediction time instant j

$$K_0(j) = [Z_{uu}(j)]^{-1},\ j=k,\ldots,k+N-1. \tag{43}$$

Moreover, when the constraint is active, calculate the optimal Lagrange multiplier variation $[\delta\mu^{(i)}(k),\delta\mu^{(i)}(k+1),\ldots,\delta\mu^{(i)}(k+N-1)]$ corresponding to initial state variation $\delta x^{(i)}(k)$ as follows:

$$\delta\mu^{(i)}(j) = -[0\ I]K_0(j) \times \begin{bmatrix} Z_{ux}(j)\delta x^{(i)}(j) + f_u^T(j)T(j+1) + H_u(j) \\ E_x^a(j)\delta x^{(i)}(j) \end{bmatrix}. \tag{44}$$

All matrices are evaluated at $x^{(i)}(\cdot)$ and $u^{(i)}(\cdot)$.

4) Find the smallest α_i among α_{ik} such that the perturbation $\alpha_i\delta x^{(i)}(k)$ changes the status of the constraint at least at one instant, namely

$$\alpha_i = \min_k\{\alpha_{ik}, k=0,\ldots,N-1, \text{and } 0\le\alpha_{ik}\le 1\}.$$

If for all $k\in[0:N-1]$, either $\alpha_{ik}<0$ or $\alpha_{ik}>1$, set $\alpha_i=1$.

5) If $\alpha_i=1$, set

$$\begin{aligned} u^{i+1}(\cdot) &= u^i(\cdot) + \delta u^{(i)}(\cdot) \\ x^{i+1}(\cdot) &= x^i(\cdot) + \delta x^{(i)}(\cdot) \end{aligned} \tag{45}$$

and set the solution $\mathbf{u}^*(x(k)) = u^{(i+1)}(\cdot)$. Otherwise:

a) if $\alpha_i=0$, change the activity status of the corresponding constraint accordingly. That is, if α_i corresponds an active (inactive) constraint, set the constraint inactive (active). Go to step 2;
b) if $\alpha_i<1$ set

$$\begin{aligned} u^{i+1}(\cdot) &= u^i(\cdot) + \alpha_i\delta u^{(i)}(\cdot) \\ x^{i+1}(\cdot) &= x^i(\cdot) + \alpha_i\delta x^{(i)}(\cdot) \end{aligned} \tag{46}$$

and

$$\begin{aligned} \delta x^{(i+1)}(k) &= (1-\alpha_i)\delta x^{(i)}(k) \\ x^{i+1}(k) &= x^i(k) + \alpha_i\delta x^{(i)}(k) \\ i &= i+1. \end{aligned}$$

Go to step 3.

Fig. 9 shows the flowchart of the InPA-SQP algorithm. The perturbed optimal control solution corresponding to the large

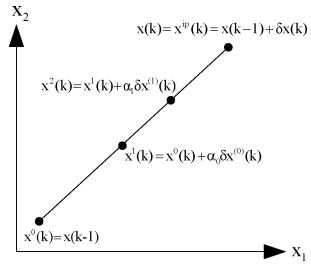

Fig. 9. Flowchart of the InPA-SQP algorithm.

perturbation $\delta x(k)$ can be approximated by augmenting the nominal solution with the intermediate ones as

$$u^*(j;x(k)) + \sum_i \delta u^{(i)}(j),\ j = k, \ldots, k+N-1.$$

If at the point $x(k)+\delta x(k)$, $\sum_{j=k}^{k+N-1} \|H_u(j)\|$ is not small enough, the prescribed procedure goes on with zero initial state perturbation $\delta x^{(i)}(k) = 0$ until the optimal solution with $\sum_{j=k}^{N+k-1} \|H_u(j)\| \simeq 0$ is achieved.

The InPA-SQP synergistically combines the solutions derived using perturbation analysis and SQP to solve the optimization problem with mixed input and state constraints. It is shown in [26] that it can significantly improve the computational efficiency while effectively handling the nonlinear constraints, making the MPC feasible for power electronics systems with fast dynamics. With the introduction of the InPA-SQP solver, we now proceed to implement the MPC on our hardware.

VI. Experimental Validation

The goal of this section is to present the experimental results to validate the effectiveness of the MPC controller using the InPA-SQP as the optimization solver.

A. Experimental Setup

Fig. 10 demonstrates a dc hybrid power system testbed which includes RT-LAB system, power converters, power sources and electronic loads. Fig. 10 shows the full bridge dc–dc converter (dc–dc1) under investigation, and it delivers power from power source to load (marked as power source1 and load1, respectively, in Fig. 10). The RT-LAB system is a PC cluster-based platform that can perform real-time simulation, hardware in the loop test and rapid control prototyping for large-scale systems. For this work, the RT-LAB system serves the following three functions: 1) as the real-time simulator to control the programmable power source1 such that it emulates the behavior of a PEM fuel cell; 2) as the rapid control prototyping unit to generate the 10 kHz modulation signals for the full bridge dc–dc converter according to MPC algorithm[1] and feedback signals; and 3) as the data acquisition device to acquire and store experimental data to enable detailed offline analysis. Note that we only use one target (Target1) in this application although our RT-LAB system has four targets. Parameters of the full bridge dc–dc converter are shown in Table I.

[1]The algorithm was first compiled with a host PC, which is connected to the RT-LAB target used to control the power converter. Then, the generated C code is downloaded and executed in the target to control the power converter.

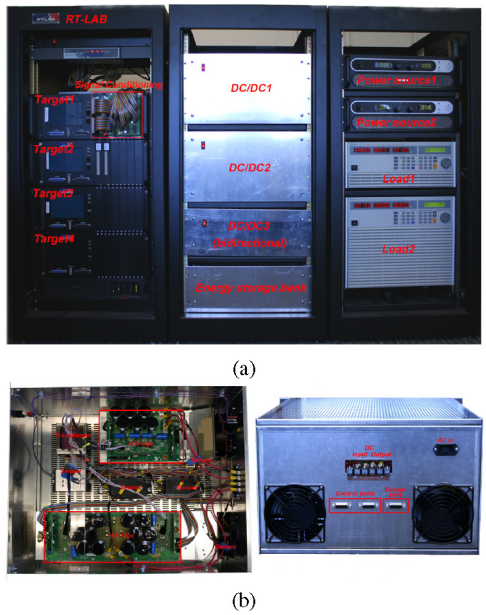

Fig. 10. Experimental setup. (a) DC hybrid power system testbed. (b) Full bridge dc–dc converter.

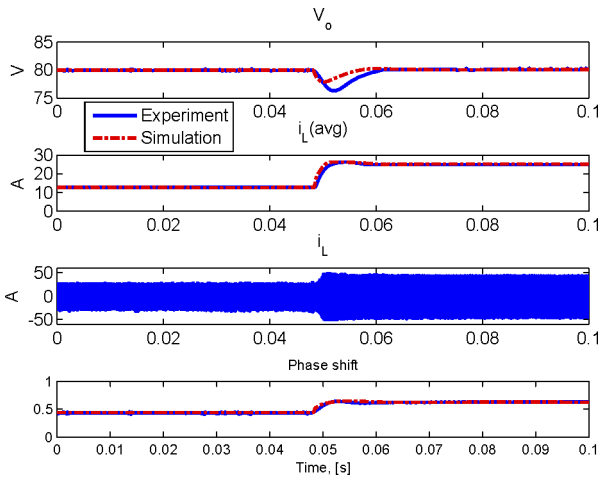

Fig. 11. Simulation and experimental waveforms for a step-down change of R from 12.8 to 6.4 $\Omega(i_L\,(\mathrm{avg}) = \bar{i}_L)$.

B. Experimental Results

First, we investigate the closed-loop performance in the presence of a large step change in the load resistance R. Fig. 11 compares the waveforms for a step-down change of R when the algorithm is applied to control the nonlinear model represented by (15)–(17) and the full bridge dc–dc converter shown in Fig. 10. Initial R is 12.8 Ω(500 W output power). A step-down change of the load resistance R is then applied to deliver 1000 W output power, which is the rated output power of the converter. The transient responses of the MPC applied to both the large signal dynamic model and the actual dc–dc converter are essentially the same. Moreover, at both load conditions, the

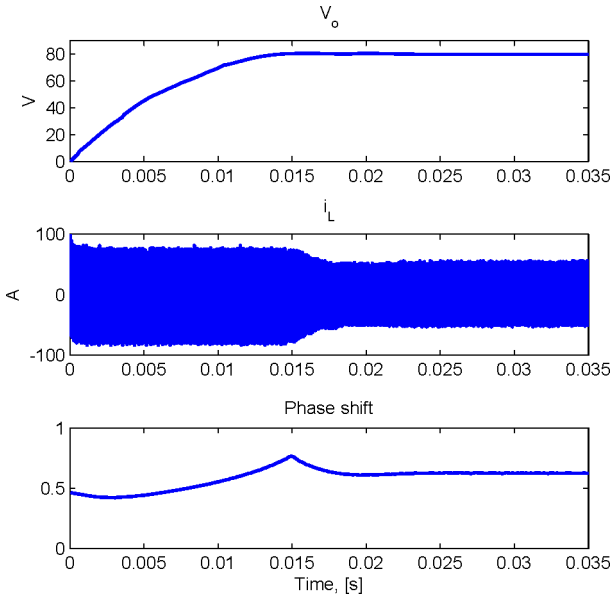

Fig. 12. Experimental waveforms for starting process with $R = 6.4\ \Omega$ (nominal).

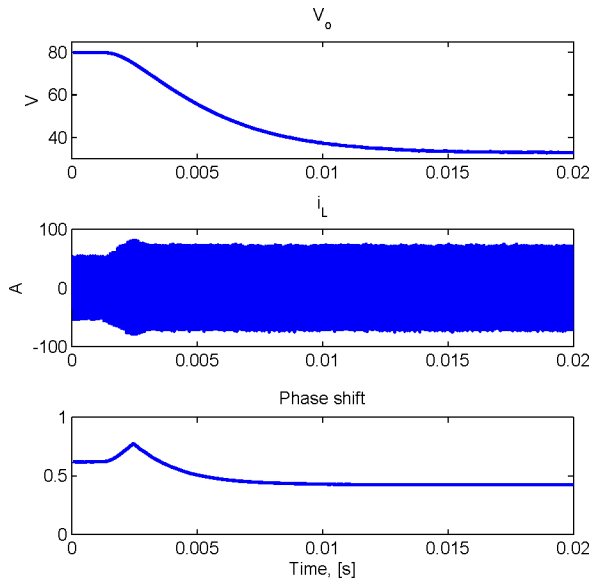

Fig. 13. Experimental waveforms for over load $R = 1.6\ \Omega$.

output voltage is regulated to the desired value, which confirms the robustness of the control scheme.

Fig. 12 shows the experimental waveforms for the starting process. The peak current is limited within the maximum tolerable value 75 A while the output voltage is regulated to 80 V. From the third plot, the phase shift (control input) first hits the nonlinear constraint and then is constrained by the upper limit during the starting process.

Finally, Fig. 13 shows the experimental waveforms for the over load case. During the steady state, the peak current is limited within the maximum tolerable value 75 A although the peak current is slightly higher than 75 A for about 1 ms during the transient. This is partially due to the fact that we do not use a current sensor in the control scheme. The output voltage drops from 80 to 32 V during the transient since i_L is constrained. From the third plot, the phase shift (control input) first hits the upper limit and then is constrained to remain within the peak current limit. No overrun is observed in any these tests.

The results reveal that the MPC controller successfully achieves voltage regulation and peak current protection. The successful implementation of MPC in real-time verifies that the InPA-SQP can significantly improve computational efficiency while gracefully handling the nonlinear constraint. Therefore, it is feasible to apply implicit MPC for fast dynamic systems such as the power electronics system, if the InPA-SQP solver is applied.

VII. Conclusion

In this paper, we analyzed the operation of the full bridge dc–dc converter. Based on the analysis, a large signal dynamic model for the full bridge dc–dc converter was developed. We formulated the voltage regulation problem of the converter in the context of MPC, where the peak current protection requirement was considered as a mixed state and input constraint. To achieve sub-millisecond level sampling time and simultaneously handle the nonlinear constraint, the InPA-SQP method was introduced to solve the constrained optimal control problem. The InPA-SQP solver can meet the computational efficiency demand while handling the nonlinear constraint. The effectiveness of the proposed control algorithm, including the peak current protection capability, has been verified with experimental results.

References

[1] J. Larminie and A. Dicks, *Fuel Cell Systems Explained*, 2nd ed. New York: Wiley, 2003.

[2] R. W. De Doneker, D. M. Divan, and M. H. Kheraluwala, "A three-phase soft-switched high-power-density dc/dc converter for high-power applications," *IEEE Trans. Ind. Appl.*, vol. 27, no. 1, pp. 797–806, Jan./Feb. 1991.

[3] M. H. Kheraluwala, R. W. Gascoigne, D. M. Divan, and E. D. Baumann, "Performance characterization of a high-power dual active bridge dc-to-dc converter," *IEEE Trans. Ind. Appl.*, vol. 28, no. 6, pp. 1294–1301, Nov./Dec. 1992.

[4] Y. Xie, G. Seenumani, J. Sun, Y. Liu, and Z. Li, "A PC-cluster based real-time simulator for all electric ship integrated power systems analysis and optimization," in *Proc. IEEE Electr. Ship Technol. Symp. (ESTS)*, 2007, pp. 396–401.

[5] K. P. Adzakpa, K. Agbossou, Y. Dube, M. Dostie, M. Fournier, and A. Poulin, "PEM fuel cells modeling and analysis through current and voltage transient behaviors," *IEEE Trans. Energy Convers.*, vol. 23, no. 2, pp. 581–591, Jun. 2008.

[6] J. T. Pukrushpan, A. G. Stefanopoulou, and H. Peng, *Control of Fuel Cell Power Systems: Principles, Modeling, Analysis and Feedback Design*. Berlin, Germany: Springer-Verlag, 2004.

[7] V. Tsourapas, A. Stefanopoulou, and J. Sun, "Model-based control of an integrated fuel cell and fuel processor with exhaust heat recirculation," *IEEE Trans. Control Syst. Technol.*, vol. 15, no. 2, pp. 233–245, Mar. 2007.

[8] J. Sun and I. Kolmanovsky, "Robust reference governor for fuel cell starvation protection," *IEEE Trans. Control Syst. Technol.*, vol. 13, no. 6, pp. 911–920, Nov. 2005.

[9] S. Chattopadhyay and S. Das, "A digital current-mode control technique for DC-DC converters," *IEEE Trans. Power Electron.*, vol. 21, no. 6, pp. 1718–1726, Nov. 2006.

[10] M. Chen, A. Mathew, and J. Sun, "Nonlinear current control of single-phase PFC converters," *IEEE Trans. Power Electron.*, vol. 18, no. 6, pp. 2187–2194, Nov. 2007.

[11] Y. Lu, K. W. E. Cheng, and S. L. Ho, "Quasi current mode control for the phase-shifted series resonant converter," *IEEE Trans. Power Electron.*, vol. 23, no. 1, pp. 353–358, Jan. 2008.
[12] J. Sun and M. Chen, "Nonlinear average current control using partial current measurement," *IEEE Trans. Power Electron.*, vol. 23, no. 4, pp. 1641–1648, Jul. 2008.
[13] R. Redl and I. Novak, "Instabilities in current-mode controlled switching voltage regulators," in *Proc. IEEE Power Electron. Spec. Conf. (PESC)*, 1981, pp. 17–28.
[14] P. Cortes, M. P. Kazmierkowski, R. M. Kennel, D. E. Quevedo, and J. Rodriguez, "Predictive control in power electronics and drives," *IEEE Trans. Ind. Electron.*, vol. 55, no. 12, pp. 4312–4324, Dec. 2008.
[15] P. Cortes, J. Rodriguez, D. E. Quevedo, and C. Silva, "Predictive current control strategy with imposed load current spectrum," *IEEE Trans. Power Electron.*, vol. 23, no. 2, pp. 612–618, Mar. 2008.
[16] T. Geyer, G. Papafotiou, and M. Morari, "Model predictive direct torque control—Part I: Concept, algorithm, and analysis," *IEEE Trans. Ind. Electron.*, vol. 56, no. 6, pp. 1894–1905, Jun. 2009.
[17] T. Geyer, G. Papafotiou, and M. Morari, "Model predictive direct torque control—Part II: Implementation and experimental evaluation," *IEEE Trans. Ind. Electron.*, vol. 56, no. 6, pp. 1906–1915, Jun. 2009.
[18] E. I. Silva, B. P. McGrath, D. E. Quevedo, and G. C. Goodwin, "Predictive control of a flying capacitor converter," in *Proc. Amer. Control Conf.*, 2007, pp. 3763–3768.
[19] S. Qin and T. Badgwell, "A survey of industrial model predictive control technology," *Control Eng. Pract.*, vol. 11, pp. 733–764, 2003.
[20] D. Q. Mayne, J. B. Rawlings, C. V. Rao, and P. O. M. Scokaert, "Constrained model predictive control: stability and optimality," *Automatica*, vol. 36, pp. 789–814, Jun. 2000.
[21] M. Morari and J. Lee, "Model predictive control: Past, present and future," *Comput. Chem. Eng.*, vol. 23, pp. 667–682, 1999.
[22] A. Bemporad, M. Morari, V. Dua, and E. N. Pistikopoulos, "The explicit linear quadratic regulator for constrained systems," *Automatica*, vol. 38, pp. 3–20, Jan. 2002.
[23] P. TØndel, T. A. Johansen, and A. Bemporad, "An algorithm for multi-parametric quadratic programming and explicit MPC solutions," *Automatica*, vol. 39, pp. 489–497, Mar. 2003.
[24] T. Geyer, G. Papafotiou, and M. Morari, "Hybrid model predictive control of the step-down DC-DC converter," *IEEE Trans. Control Syst. Technol.*, vol. 16, no. 6, pp. 1112–1124, Nov. 2008.
[25] Y. Wang and S. Boyd, "Fast model predictive control using online optimization,," in *Proc. 17th IFAC World Congr.*, 2008, pp. 6974–6997.
[26] R. Ghaemi, J. Sun, and I. Kolmanovsky, "Model predictive control for constrained discrete time systems: An optimal perturbation analysis approach," in *Proc. Amer. Control Conf.*, 2007, pp. 3757–3762.
[27] R. Ghaemi, J. Sun, and I. Kolmanovsky, "An integrated perturbation analysis and sequential quadratic programming approach for model predictive control," *Automatica*, vol. 45, pp. 2412–2418, Sep. 2009.
[28] F. Z. Peng, M. Shen, and K. Holland, "Application of Z-source inverter for traction drive of fuel cell-battery hybrid electric vehicles," *IEEE Trans. Power Electron.*, vol. 22, no. 3, pp. 1054–1061, May 2007.
[29] C. Mi, H. Bai, C. Wang, and S. Gargies, "Operation, design and control of dual H-bridge-based isolated bidirectional DC–DC converter," *IET Power Electron.*, vol. 1, pp. 507–517, Dec. 2008.
[30] C. Zhao, X. Wu, P. Meng, and Z. Qian, "Optimum design consideration and implementation of a novel synchronous rectified soft-switched phase-shift full-bridge converter for low-output-voltage high-output-current applications," *IEEE Trans. Power Electron.*, vol. 24, no. 2, pp. 388–397, Feb. 2009.
[31] J. Sun and H. Grotstollen, "Averaged modelling of switching power converters: Reformulation and theoretical basis," in *Proc. IEEE Appl. Power Electron. Conf. Expo. (APEC)*, 1992, pp. 1165–1172.
[32] J. Sun, D. M. Mitchell, M. F. Greuel, P. T. Krein, and R. M. Bass, "Averaged modeling of PWM converters operating in discontinuous conduction mode," *IEEE Trans. Power Electron.*, vol. 16, no. 4, pp. 482–492, Jul. 2001.
[33] A. Davoudi, J. Jatskevich, and T. De Rybel, "Numerical state-space average-value modeling of PWM DC–DC converters operating in DCM and CCM," *IEEE Trans. Power Electron.*, vol. 21, no. 4, pp. 1003–1012, Jul. 2006.
[34] W. S. Levine, *The Control Handbook*. Boca Raton, FL/Piscataway, NJ: CRC Press/IEEE Press, 1996.

Yanhui Xie (S'09–M'09–SM'09) received the M.S. degree in electrical engineering from Shanghai Jiao Tong University, Shanghai, China, in 2003. He is currently working toward the Ph.D. degree at the Department of Naval Architecture and Marine Engineering, University of Michigan, Ann Arbor.

From 2002 to 2004, he was a Power Electronics Research and Development Engineer, Shanghai Research and Development Center of TDK-LAMBDA Corporation, Shanghai, China. His current research interests include design, integration, modeling and advanced control of energy storage, power conversion, and motor drive systems.

Reza Ghaemi received the B.S. and M.S. degrees from the University of Tehran, Tehran, Iran, in 1998 and 2001, respectively.

From 2001 to 2004, he conducted research on control and monitoring of power electronic systems at the Power Research Institute, Tehran. He is currently a Graduate Research Assistant with the Department of Electrical Engineering and Computer Science, University of Michigan, Ann Arbor. His research interests include optimal control theory and model predictive control.

Jing Sun (S'87–M'89–SM'00–F'04) received the B.S. and M.S. degrees from the University of Science and Technology of China, Hefei, China, in 1982 and 1984, respectively, and the Ph.D. degree from the University of Southern California, Los Angeles, CA, in 1989.

From 1989 to 1993, she was an Assistant Professor with the Electrical and Computer Engineering Department, Wayne State University, Detroit, MI. She was with the Powertrain Control Systems Department, Ford Research Laboratory, Dearborn, MI, during 1993. In 2003, she joined the Faculty of the College of Engineering, University of Michigan, where she is currently a Professor with the Department of Naval Architecture and Marine Engineering and Department of Electrical Engineering and Computer Science. Her current research interests include system and control theory and its applications to marine and automotive propulsion systems. She holds over 30 US patents and is the coauthor of a textbook on *Robust Adaptive Control*.

Dr. Sun is one of the three recipients of the 2003 IEEE Control System Technology Award.

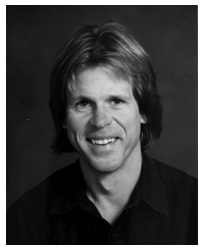

James S. Freudenberg (S'80–M'84–SM'97–F'00) received the B.S. degree in mathematics and physics from the Rose-Hulman Institute of Technology, Terre Haute, IN, in 1978, and the M.S. and Ph.D. degrees in electrical engineering from the University of Illinois, Urbana-Champaign, in 1982 and 1985, respectively.

He is currently a full-time Professor with the Department of Electrical Engineering and Computer Science, University of Michigan, Ann Arbor. His current research interests include the theory of fundamental limitations and the teaching of embedded control systems.